Active flow control of a two-dimensional compressible cavity flow using direct output feedback law

Christophe Airiau

Institut de Mécanique des Fluides de Toulouse

RAPPORT D'ACTIVITE POUR LA FRAE

Projet ECOSEA

Estimation, **CO**ntrôle et **S**tabilisation d'**E**coulements **A**érodynamique

---

Active flow control
of a two-dimensional compressible cavity flow using direct output feedback law

Pr Christophe Airiau

Christophe.Airiau@imft.fr

Institut de Mécanique des Fluides de Toulouse,
allée du professeur Camille Soula,
31400 Toulouse

Rapport intermédiaire et définitif

30 septembre 2013

Contents

List of Figures

Abstracts

Résumé

Les perturbations acoustiques présentes dans un écoulement de cavité bidimensionnel et compressible sont analysées et contrôlées au moyen de simulations numériques directes (DNS) et d'une loi de rétroaction en retour de sortie liant l'actionneur de type jet synthétique à des prises de pression pariétales. La loi de contrôle est obtenue en bâtissant un modèle réduit dynamique non linéaire de l'écoulement non contrôlé et forcé par une excitation à large spectre puis en menant une étude de contrôle actif de type "Linear Quadratic Regulator". La loi de contrle implémentée dans les DNS conduit à une réduction significative et globale des émissions acoustiques (jusqu'à 10 dB). Le contrôle reste efficace bien en dehors de la fenêtre temporelle d'observation qui a servi à l'obtention du modèle réduit. L'approche continue d'amortir les perturbations pour un contrôle de moyenne amplitude induisant des effets non linéaires.

mots clés : Contrôle; boucle fermée; écoulement compressible; réduction du bruit

Abstract

Acoustic perturbations emitted from a two dimensional compressible cavity flow are analysed and controlled using direct numerical simulations (DNS) and an output feedback law which expresses the actuation (a synthetic jet) velocity as a function of wall pressure fluctuation sensors. To get the feedback control law, a non-linear reduced-order model (ROM) is first built from un-actuated flow fields and flow forced with a large frequency bandwidth actuation. The control law is then determined by a Linear Quadratic Regulator algorithm. The control law implemented in the DNS provides a significant and global noise reduction (up to 10 dB). The actuation law remains efficient for long times, greater than the temporal window of observation used to design the ROM. Actuation of moderate amplitudes generate some non-linear effects but perturbations continue to be damped.

Keywords: Control ; feedback law ; cavity ; compressible flow ; noise reduction

Préambule

Le travail inclus dans ce rapport fait suite à l'appel d'offre "Mathématique" de la FNRAE et présente une réponse au thème 4 "Identification, détection, contrôle en propagation d'ondes".

Le projet ECOSEA se propose de traiter l'**E**stimation, le **CO**ntrôle et la **S**tabilisation d'**E**coulements **A**érodynamiques. L'équipe de l'IMFT s'est concentrée sur un écoulement classique mais riche par son contenu : une couche limite bidimensionnelle compressible, laminaire affleurant une cavité rectangulaire. Un mécanisme de rétroaction génère une instabilité auto-entrenue qui est la source d'ondes acoustiques qui se propagent dans l'écoulement. Il s'agit donc de chercher des stratégies de contrôle actif en boucle fermée qui aboutiront à une réduction significative des émissions acoustiques. Ce cas de contrôle aéroacoustique s'avère plus difficile et exigeant numériquement qu'un contrôle d'un décollement dans un fluide incompressible à relativement bas nombre de Reynolds,

Nous allons ici décrire une méthodologie qui pourra être étendue à d'autres types d'écoulements, et pour d'autres objectifs tels que la réduction de traînée ou l'augmentation de la portance. Il s'agirait alors de contrôler des ondes d'instabilités dans les couches limites ou de réduire ou supprimer les décollements de couche limite ou les recirculations de culot de corps épais.

La démarche de contrôle d'écoulements proposé est potentiellement susceptible d'apporter des améliorations dans la conception et les performances de véhicules tant terrestre, que navals et aériens.

La projet ECOSEA se proposait d'améliorer quelques points durs existants associé au contrôle en boucle fermée :

1. Les simulations numériques ou les expériences produisent des champs de vitesse, de pression ou de température de dimension N , de $N = 10^4$ à 10^8. Cette dimension ou degrés de liberté est énorme par rapport aux dimensions des problèmes rencontrés en automatique (science des systèmes), . Pour appliquer les théories des systèmes il faut donc diminuer la dimension de nos problèmes en utilisant la technique de réduction de modèle.

2. Pour améliorer un dispositif de contrôle il faut placer, autant que possible, les actionneurs et les capteurs optimalement, or leurs positions sont souvent choisies en fonction de contraintes de conception ou technologiques. Il serait donc très intéressant de connaître les positions optimales au sens mathématique du terme.

3. L'estimation de l'état en fonction de mesures de capteurs est un problème à lui seul et de nombreuses approches existent. En mécanique des fluides, on utilise principalement des estimations stochastiques linéaires ou l'approche basée sur le filtre de Kalman. Des approches plus complexes existent en automatique ou dans les problèmes d'assimilation de données qui devraient être testées pour des écoulements.

4. Le principe de séparation définie en théorie du contrôle propose de traiter séparément la partie estimation de la partie contrôle . Mais le couplage existe malgré tout. Peu de travaux portent sur une meilleure prise en compte de ce couplage, en particulier en présence de nonlinéarités.

5. Enfin, le mouvement des fluides répond au modèle des équations de Navier-Stokes qui sont fortement non linéaires. La physique même des écoulement est fortement non linéaire. La conception de la loi de con dans les problèmes non linéaires se fait très souvent autour d'un état tangent suite à une linéarisation locale. Des travaux à l'Institut de Mathématique de Toulouse ont démarré sur la conception de lois de contrôle nonlinéaires. Les résultats sont encore mitigés, mais clairement des recherches appronfondies doivent être poursuivies dans ce sens.

L'équipe de l'IMFT s'est attachée à améliorer les points 1, 2 et 3 et un peu 4. Les ressources dédiées au projet n'ont pas permis d'avancer sur le point 5.

Ce travail fait suite à de nombreuses recherches portant sur le contrôle des écoulements menées à l'IMFT dans diverses situations. La figure présente un aperçu des projets, des types de contrôle et des configurations étudiés ou en cours d'étude. En annexe D on trouve un tableau indiquantles nouvelles implémentations et les avancées obtenues ans le projet Ecosea qui suivait et chevauchait le projet ANR Cormored.

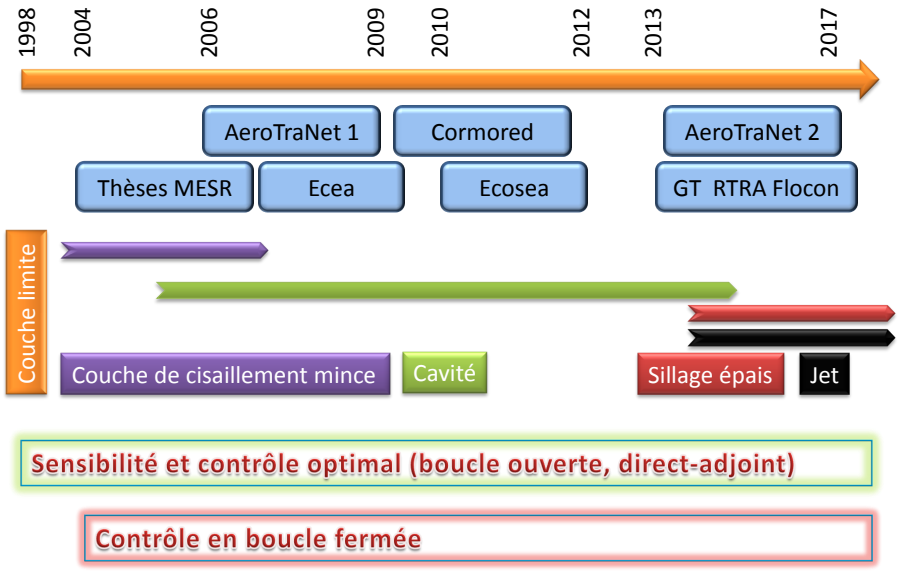

Figure 1 - *Travaux sur le contrôle des écoulements à l'IMFT*

Le premier chapître du rapport présente la méthodologie proposée, le cas test ainsi que des résultats intermédiaires pour aborder le problème de contrôle en boucle fermée sur la base de simulation numériques directes. L'accent est uniquement mis sur les points importants théoriques et parfois numériques des approches proposées. Une chaîne numérique relativement complexe a été implémentées avec des blocs de programmes en FORTRAN 90 ou en MATLAB et des communications entre blocs en langage shell BASH. Le second chapître présente les résultats de l'application de la méthodologie et l'analyse de la dynamique d'un écoulement contrôlé. On montre ainsi qu'un contrôle efficace et relativement robuste a été conçu. Le document se termine par une conclusion et propose de nouvelles pistes d'amélioration ou d'investigation. Des annexes développent quelques détails qui n'ont pas nécéssairement leur place dans le corps du rapport.

Une partie du travail a été ou sera présentée au Congrès Français de Mécanique en 2011, au congrès internationale MUSAF, à Toulouse en septembre 2013 et au workshop du GDR " contrôle du décollement " à Lille en novembre 2013. Un article dans un livre va être publié et un article est en cours de rédaction pour une revue internationale, ce qui explique que la suite du rapport est en langue anglaise.

Chapter 1

Methodology and applications

In this chapter the methodology which includes numerical tools and theories are presented. The testcase is introduced and the key point of the actuation mode determination is discussed. Some intermediaite results are displayed and analysed.

1.1 Introduction

In most of the flow configurations of practical interest, the range of spatial and temporal scales in strong interaction is so large that an accurate analysis and computation require a huge number of degrees of freedom. This issue becomes critical when the objective is to develop a model-based flow control strategy. Indeed, passive flow control is directly linked to shape optimization that is in general an iterative procedure, and active flow control is typically an unsteady approach for which we would like to act in real-time. One way of reducing the number of degrees of freedom by several orders of magnitude is to use Reduced-Order Models (ROMs) based on projection methods. Different approaches can be employed. For instance, the linear global or local stability eigenmodes of the flow can be exploited for deriving such model. However the eigenvalue problem is so large for realistic flows that this approach is very often limited by the computer resources and accuracy. But coupled with a projection method and sometimes using a Proper Orthogonal Decomposition (POD) it is possible to derive a linear balanced reduced order model which can be controlled by the linear control theory. Many applications and developments can be found in the literature [1, 4, 5]. Another approaches will define some heuristic or simple linear models from the flow physical analysis (using POD for instance) [2]. Here, we will use reduced-order model based on Proper Orthogonal Decomposition (POD) and consider for configuration a compressible cavity flow computed by Direct Numerical Simulation (DNS). In the objective to reduce flow instabilities and the level of noise emissions, we design a feedback control law between few wall pressure sensors located at strategic locations in the cavity and an actuator. A major difficulty is to introduce explicitly the control law in the ROM model obtained by Galerkin projection of the Navier-Stokes equations onto the POD modes. For that, we first determine an actuation mode from a given forced simulation. After linearization of the reduced-order model around an equilibrium state, we will determine a feedback control law from a Linear Quadratic Regulator (LQR) approach. Its efficiency and robustness are finally tested in the DNS code. The general methodology is presented on picture 1.1. The initial sensitivity study based on adjoint of the direct numerical simulations is included.

Compared to our previous studies on the subject [9, 14], some improvement have been implemented. Usually, a feedback law is a direct relation between the state of the system and the actuation as shown in figure 1.2. Here, we overpass the knowledge of the state to determine an output feedback law directly from some sensors' values (red dashed arrow of the figure 1.2). Moreover, we have changed the inner product used in the POD, modified the governing equations in the Galerkin projection and simplified the

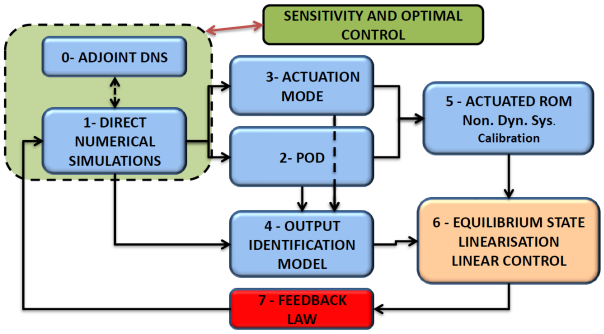

Figure 1.1 - *General methodology*

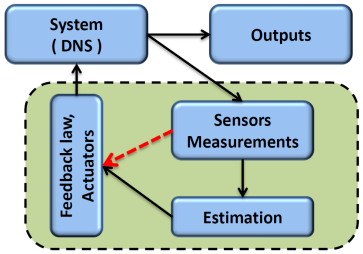

Figure 1.2 - *Direct feedback output control*

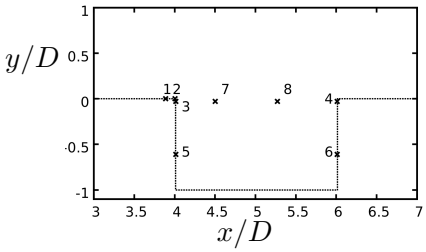

Figure 1.3 - *Sensors' locations in non dimensional variables. Numbers 7 and 8 are off.*

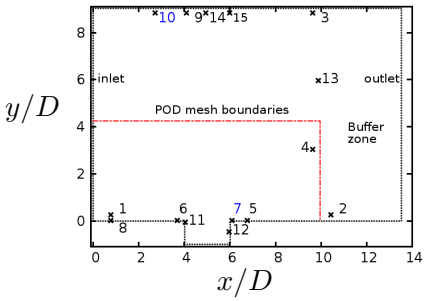

Figure 1.4 - *POD domain and probes' locations in non dimensional variables.*

linear control approach. In addition, a new identification model of the output was also introduced.

In Section 1.2, the configuration and the parameters of the direct numerical simulations are given, and the chirp actuation is described. The POD reduced-order model and the LQR strategy are discussed in Section 1.3. The feedback law is numerically tested on the DNS in Section 2. Finally, the paper ends with some perspectives.

1.2 Direct Numerical Simulations

1.2.1 Governing equations, configuration

The governing equations are the two-dimensional compressible Navier-Stokes equations written with the conservative formulation. The static pressure p is given from the ideal gas state equation. No slip boundary conditions are imposed at the wall except when actuation is on. The present reference test case is very close to one of those found in [20]. We consider a laminar boundary layer flow over a rectangular cavity of aspect ratio length/depth (L/D) equal to 2 (Figs. 1.3 and 1.4). At the upstream cavity corner, the Reynolds number based on the momentum boundary layer thickness is 188 and the Reynolds number based on L is 2982. The air upstream conditions are Mach number $M_\infty = 0.6$ and a temperature $T_\infty = 298°$K [13, 14]. This flow is well known to produce self-sustained instabilities. The impingement of the shear layer on the downstream edge of the cavity induces a pressure wave which excites the shear layer instability by a feedback mechanism. It is therefore characterized by a strong coupling between hydrodynamic instability and an acoustic wave propagation [17]. Generally, studies aim to reduce the noise emitted outside the cavity at some specific frequency approximated by the Rossiter formula. Several acoustic modes can be found depending on the state and properties of the boundary conditions and of the aspect ratio of the cavity flow. In this 2D test case, the fundamental noise frequency (see Fig. 1.5) is found at a Strouhal number $St_L = f \times L/U_\infty = 0.703$, close to the so called

second Rossiter mode given by $St_L = 0.74$.

Six unsteady pressure sensors are chosen at the cavity walls for deriving the control law (Fig. 1.3) and 15 additional probes are introduced to record the temporal evolutions of flow fields for spectral analysis (Fig. 1.4). The reference simulations are run over $N_t = 25000$ uniform time steps Δt from 0 to 22.52 where the time is nondimensionalized by the upstream sound velocity a_∞ and the cavity length L. Over this time horizon, approximately 10 Rossiter's cycles are displayed (Fig. 2.2). The DNS code (named ASIA) has been validated in various configurations. Numerical schemes, non reflecting boundary conditions and other informations are found in [13].

The simulation code (ASIA) has been validated in various configurations a [13]. An alternate fourth order Runge-Kutta scheme is used for temporal discretisation and sixth order compact schemes are used for spatial derivative discretisation [10, 11]. A non regular cartesian multi-block grid is designed to capture high gradients close to the wall. The characteristic boundary conditions are implemented to avoid acoustic wave reflections on open boundaries of the computational domain [16, 22] and a buffer region is added at the outlet of the domain to damp any residual numerical waves for $x/D > 9.96$ (Fig. 1.4). Some ghost cells are introduced into the mesh to avoid any wall point to be a computed grid node.

1.2.2 Chirp actuation

For introducing explicitly the control term in the POD model, at least one actuation mode must be determined from a forced simulation. The results will strongly depend on the actuation law imposed in this simulation. The location of the forcing and its type (direction, physical quantity) have been set after a numerical sensitivity analysis of the pressure field to different types of forcing using adjoint DNS of the Navier-Stokes equations [3, 13, 21]. The actuator is finally centered close to the upstream edge of the cavity at $x/D \approx 3.6$ that corresponds to the highest sensitivity zone, and the action is on the normal velocity at the wall simulating a blowing/suction effect. From the sensitivity analysis, we impose a spatial Gaussian distribution actuation law on a small wall slot of width 15 streamwise steps Δx, centered on a given location $\boldsymbol{x}_0$:

$$\mathbf{f}_w(\boldsymbol{x}, t) = \gamma(t) \exp(- \frac{||\boldsymbol{x} - \boldsymbol{x}_0||^2}{\sigma^2}), \qquad \sigma = f(\Delta x)$$

To excite a large bandwidth of flow frequencies, we impose for forcing term $\gamma(t)$ a slowly varying amplitude and frequency called chirp actuation and given by:

$$\gamma(t) = A_1 \sin(2\pi St_1\, t) \times \sin\left(2\pi St_2\, t - A_2 \sin(2\pi St_3\, t)\right). \tag{1.1}$$

The non-dimensional amplitude A_1 governs the linear effect of the perturbation with respect to a given time mean field. The other parameters control the large time variation of the phase, the frequency and the amplitude. We set $A_2 = 27$, $St_1 = 1/30$, $St_2 = 2/15$ and $St_3 = 8/3$ (reference time L/a_∞). An analytical forcing as equation (1.1) is preferred, even if not necessary, to a white noise because this equation is used for the identification model of outputs and in the calculus of the actuation mode. As displayed in Fig. 1.6, the range of Strouhal numbers covered by the chirp excitation is large and includes the second Rossiter mode ($St \approx 0.7$) and its harmonics. The more the amplitude A_1 increases, the more the non-linear effects become dominant in the flow. In the following, A_1 is hence set to 0.01 of the upstream velocity U_∞ to keep approximately linearity and to produce an observable and significant effect.

When actuation is one at the wall, the velocity, pressure and energy boundary conditions are modified. Since the actuation is localized in a small wall length, no nonreflective boundary conditions are required, and no numerical wave reflection are observed as shown in section 2.

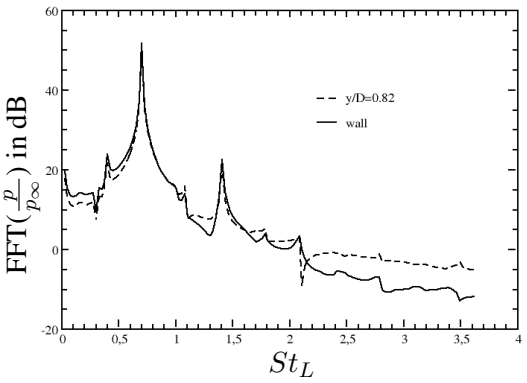

Figure 1.5 - *Spectrum of the uncontrolled flow at $x/D = 3.33$. FFT done over 75000 time steps.*

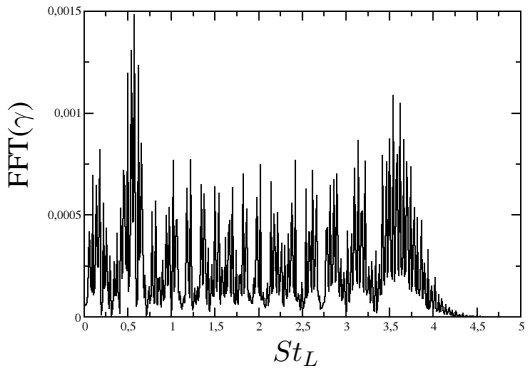

Figure 1.6 - *FFT over 100 000 time steps of the chirp actuation.*

1.3 Reduced Order Modelling

1.3.1 Proper Orthogonal Decomposition and actuation mode

Let $\boldsymbol{q}(\boldsymbol{x}, t)$ be the state variables, and $\boldsymbol{x}$ denotes the location vector (x, y). Proper Orthogonal Decomposition [15] is performed over a reduced space domain centered on the cavity (see Fig. 1.4). For that, 250 snapshots sampled every 100 time steps of the numerical simulations are considered for the snapshot POD algorithm. Here, we choose an inner product weighted by the inverse of the variance of each state variable component as in [6] (cf. Appendix A)

For an un-actuated flow (variables with superscript u), the POD expansion reads

$$\boldsymbol{q}^{\mathrm{u}}(\boldsymbol{x}, t) = \bar{\boldsymbol{q}}^{\mathrm{u}}(\boldsymbol{x}) + \sum_{i=1}^{N} a_i^{\mathrm{u}}(t)\boldsymbol{\phi}_i^{\mathrm{u}}(\boldsymbol{x}) \tag{1.2}$$

where $\bar{\boldsymbol{q}}^{\mathrm{u}}(\boldsymbol{x})$ is the mean time flow, $\boldsymbol{\phi}_i^{\mathrm{u}}(\boldsymbol{x})$ are the POD modes and $a_i^{\mathrm{u}}(t)$ the mode coefficients. For representing the actuated flows (superscript a), an actuation mode $\boldsymbol{\psi}(\boldsymbol{x})$ is added to the previous un-actuated expansion leading to

$$\boldsymbol{q}^{\mathrm{a}}(\boldsymbol{x}, t) = \bar{\boldsymbol{q}}^{\mathrm{a}}(\boldsymbol{x}) + \sum_{i=1}^{N} a_i^{\mathrm{a}}(t)\boldsymbol{\phi}_i^{\mathrm{u}}(\boldsymbol{x}) + \gamma(t)\boldsymbol{\psi}(\boldsymbol{x}), \tag{1.3}$$

where $\gamma(t)$ is the control parameter. The actuation mode is determined from the snapshots obtained in section 1.2.2 for the chirp actuation (see [9, 14]). By construction, $\boldsymbol{\psi}(\boldsymbol{x})$ is orthogonal to the un-actuated POD modes $\boldsymbol{\phi}_i^{\mathrm{u}}(\boldsymbol{x})$ following the simple algorithm :

1. $a_i^{\mathrm{a}}(t) = \langle \boldsymbol{q}^{\mathrm{a}}(\boldsymbol{x}, t) - \bar{\boldsymbol{q}}^{\mathrm{a}}(\boldsymbol{x}), \boldsymbol{\phi}_i^{\mathrm{u}}(\boldsymbol{x}) \rangle_\Omega$
2. $\boldsymbol{\psi}(\boldsymbol{x}) = \langle \boldsymbol{q}^{\mathrm{a}}(\boldsymbol{x}, t) - \bar{\boldsymbol{q}}^{\mathrm{a}}(\boldsymbol{x}) - \sum_{i=1}^{N} a_i^{\mathrm{a}}(t)\boldsymbol{\phi}_i^{\mathrm{u}}(\boldsymbol{x}), \gamma(t) \rangle_t \; / \; \langle \gamma(t), \gamma(t) \rangle_t$

The index Ω and t in the inner products denotes respectively the spatial and temporal inner products. The expansion (1.3) is based on the assumption that the mean flow is approximately not changed by the actuation i.e. $\bar{\boldsymbol{q}}^{\mathrm{a}}(\boldsymbol{x}) \approx \bar{\boldsymbol{q}}^{\mathrm{u}}(\boldsymbol{x})$. In our case, 6 POD modes are seen to be sufficient to represent the energetic content of the flow.

The figure 1.7 show the streamwise velocity component of the actuation mode ϕ^u when the reference forcing is a sine fonction. The mode is localized in space in the wall boundary layers and in the shear

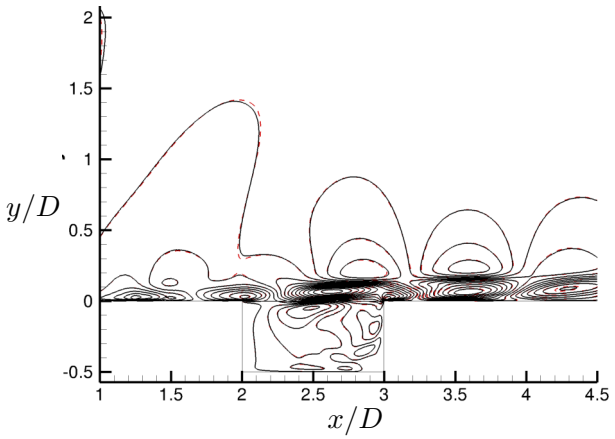

Figure 1.7 - *u velocity of the actuation mode with a sine forcing*

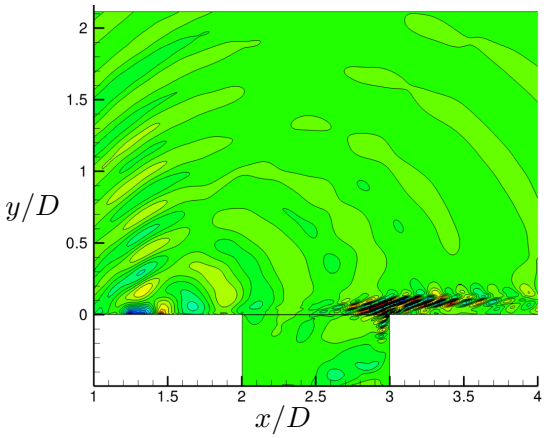

Figure 1.8 - *u velocity of the actuation mode with a chirp forcing* ($A_1 = 0.001$)

layer. The dashed red lines show the same actuation mode when another spatial inner product based on the total energy to get the correlation matrix is used for the POD determination. It indicates that the inner product definition does not play an important role. The figure 1.8 shows the same actuation with a chirp forcing. We guest the location of the actuation at the wall, upstream the cavity. We also clearly see some spatial localized structures around the downstream cavity corner, which is the source of the noise emission related to the Rossiter feedback mechanism. The actuation mode seems to have well captured the intrinsic physic of the flow and the place where to modify the flow characteristics. The response of the flow to a large bandwith frequency signal appears therefore more convenient from a control view point than a simple one frequency forcing. Because of its large bandwith frequency, more flow modes are excited and finaly the actuation mode is spatially localized close to the origin of the noise emission, at the downstream corner of the cavity. We can recognize as well the location of the forcing upstream the cavity.

1.3.2 Galerkin projection and ROM

The Reduced Order Model (ROM) of the cavity flow is obtained by a Galerkin projection of the compressible Navier-Stokes equations onto the spatial POD modes. To avoid cubic terms in the dynamical model, we have used the same formulation of the governing equations as in [6, 23], i.e.

$$\begin{aligned}
\zeta_t &= \zeta(u_x + v_y) - u\zeta_x - v\zeta_y \\
u_t &= -uu_x - vu_y - \zeta p_x + \frac{1}{Re}\zeta\left[\left(\frac{4}{3}u_x - \frac{2}{3}v_y\right)_x + (v_x + u_y)_y\right] \\
v_t &= -uv_x - vv_y - \zeta p_y + \frac{1}{Re}\zeta\left[\left(\frac{4}{3}v_y - \frac{2}{3}u_x\right)_y + (v_x + u_y)_x\right] \\
p_t &= -up_x - vp_y - \gamma p(u_x + v_y) + \frac{\gamma}{RePr}[(p\zeta)_{xx} + (p\zeta)_{yy}] \\
&+ \frac{\gamma - 1}{Re}\left[u_x\left(\frac{4}{3}u_x - \frac{2}{3}v_y\right) + v_y\left(\frac{4}{3}v_y - \frac{2}{3}u_x\right) + (v_x + u_y)^2\right]
\end{aligned} \tag{1.4}$$

where $\zeta = 1/\rho$, and u, v and p are the velocity components and pressure, respectively. In (1.4), Pr and Re denote the reference Prandtl and Reynolds numbers.

By introduction of (1.3) into (1.4), and by projection on the POD modes, a non linear dynamical system of size N is determined for $\boldsymbol{a}(t)$:

$$\dot{\boldsymbol{a}} = C + L\boldsymbol{a} + \boldsymbol{a}^T Q\boldsymbol{a} + \gamma\hat{C} + \gamma\hat{L}\boldsymbol{a} + \gamma^2\hat{Q}, \tag{1.5}$$

where the superscript T denotes the transpose. The coefficients of this reduced-order model depend on the mean flow, on the POD modes and on the actuation mode. The analytical expressions of the coefficients are given in an appendix B. It is now well known that reduced-order models derived by the traditional POD Galerkin approach may be fragile when used for control design [7]. For this reason, we calibrate the coefficients C, L, Q of the un-actuated model (1.5) using similar numerical methods as those described in [14]. Moreover, we checked for different values of the control parameter that the dynamical description of (1.5) remains satisfactory when the forcing was introduced. Some comparisons are shown in an appendix C.

The first step in the design of a feedback control law by the LQR analysis is to linearize the reduced-order model (1.5) around an equilibrium point, $\boldsymbol{a}^{\mathrm{e}}$, the steady solution of (1.5). The corresponding equilibrium state $\boldsymbol{q}^{\mathrm{e}}(\boldsymbol{x})$ is computed for the un-actuated system (1.5) with a Newton iterative algorithm. The resulting reduced-order model in the new set of coordinates $\tilde{\boldsymbol{a}} = \boldsymbol{a} - \boldsymbol{a}^{\mathrm{e}}$ is:

$$\dot{\tilde{\boldsymbol{a}}} = L\tilde{\boldsymbol{a}} + \tilde{\boldsymbol{a}}^T Q\boldsymbol{a} + \boldsymbol{a}^T Q\tilde{\boldsymbol{a}} + (\hat{C} + \hat{L}\boldsymbol{a})\gamma = \tilde{A}\tilde{\boldsymbol{a}} + \tilde{B}\gamma. \tag{1.6}$$

1.3.3 Identification model of outputs

When the mode coefficients $\boldsymbol{a}$ of (1.6) are not available, an estimation based directly on real-time measurements of surface pressure at a small number $N_s = 6$ of locations is derived. Let $\boldsymbol{y}(t)$ be the pressure measurements, the objective is to determine the model $\hat{\boldsymbol{y}}(t) = \tilde{C}\boldsymbol{a}(t) + \tilde{D}\gamma(t)$ where $\hat{\boldsymbol{y}}(t) = \boldsymbol{y}(t) - \bar{\boldsymbol{y}}$. The matrix $\tilde{C}$ and the vector $\tilde{D}$ are determined by linear stochastic estimation (LSE) and results are simply obtained by exploiting the orthogonality property of the augmented basis $(\{\boldsymbol{\phi}_i\}_{i=1}^N, \boldsymbol{\psi})$ [14]. By considering that each sensor y_i is located on the POD mesh at a position $\boldsymbol{x}_k$ it can be demonstrated that $\tilde{C}_{ij} = \phi_j^{\mathrm{u}}(\boldsymbol{x}_k)$ and $\tilde{D}_i = \boldsymbol{\psi}^p(\boldsymbol{x}_k)$, where $\boldsymbol{\psi}^p$ is the pressure component of the actuation mode. If the sensors are not located on the POD grid, a projection gives

$$\tilde{C}_{ij} = \frac{\langle \tilde{y}_i^{\mathrm{u}}, a_j^{\mathrm{u}} \rangle_t}{\langle a_j^{\mathrm{u}}, a_j^{\mathrm{u}} \rangle_t} \quad \text{and} \quad \tilde{D}_i = \frac{\langle y_i^{\mathrm{a}} - y_i^{\mathrm{u}} - \tilde{C}_{ij}(a_j^{\mathrm{a}} - a_j^{\mathrm{u}}), \gamma \rangle_t}{\langle \gamma, \gamma \rangle_t}$$

where $\langle a, b \rangle_t = \int_0^T a(t)b(t)\,\mathrm{dt}$. Finally, introducing $\tilde{\boldsymbol{y}} = \hat{\boldsymbol{y}} - \tilde{C}\boldsymbol{a}^{\mathrm{e}}$ we find the output identification model:

$$\tilde{\boldsymbol{y}} = \tilde{C}\tilde{\boldsymbol{a}} + \tilde{D}\gamma. \tag{1.7}$$

1.3.4 Linear Quadratic Regulator and output feedback control

The LQR design of the system (1.6) and (1.7) computes the gain matrix K_c, such that the state-feedback law

$$\gamma(t) = -K_c\,\tilde{\boldsymbol{a}}(t) \tag{1.8}$$

minimizes the quadratic cost function given by $\mathcal{J} = \displaystyle\int_0^{T_h} \left(\tilde{\boldsymbol{a}}^T\tilde{\boldsymbol{a}} + \ell^2\gamma^2\right)\,\mathrm{dt}$ where ℓ is a penalization term corresponding to the control cost. When the value of ℓ is high, the best possible stabilization is obtained but for an expensive cost. For an infinite time horizon ($T_h \to \infty$), the control gain is given by $K_c = \frac{1}{\ell^2}\tilde{B}^T X$, where X is solution of the continuous time algebraic Riccati equation $\tilde{A}^T X + X\tilde{A} - \frac{1}{\ell^2}X\tilde{B}\tilde{B}^T X + Id = 0$.

By manipulating (1.7) and (1.8), we can obtain an expression for γ. If the number of Galerkin POD modes N is equal to the number of sensors N_s then

$$\gamma(t) = -K_c(\tilde{C} - \tilde{D}K_c)^{-1}(\boldsymbol{y} - \bar{\boldsymbol{y}} - \tilde{C}\boldsymbol{a}^{\mathrm{e}}).$$

Otherwise, we use the pseudoinverse and find

$$\gamma(t) = -K_c[(\tilde{C} - \tilde{D}K_c)^T(\tilde{C} - \tilde{D}K_c)]^{-1}(\tilde{C} - \tilde{D}K_c)^T(\boldsymbol{y} - \bar{\boldsymbol{y}} - \tilde{C}\boldsymbol{a}^{\mathrm{e}}).$$

In summary, the direct output feedback control law reads:

$$\gamma(t) = \boldsymbol{\alpha}^T(\boldsymbol{y}(t) - \bar{\boldsymbol{y}}) + \beta, \tag{1.9}$$

where $\boldsymbol{\alpha}$ is a vector of dimension N_s and $\beta = -\boldsymbol{\alpha}^T\tilde{C}\boldsymbol{a}^{\mathrm{e}}$ is a real number. From equation (1.9) which is a linear relationship between the actuation and the outputs, β governs the level of the steady part of the actuation while the $\boldsymbol{\alpha}$ vector governes the damping rate of the unsteady part of the actuation.

1.4 First conclusions

On the based of a reduced order model and of a Linear Quadratic Regulator control approach, it is possible to design an actuation feedback law from sensors signal suitly located in the flow. An important issue is to generate some flow fields in known actuated conditions in order to well capture and to model an actuated mode which is a RHS forcing term of a nonlinear dynamical system.

Another important point is that the actuation low is linear with respect to the fluctuated pressure and the sum of a damping term and a constante velocity. Because of its simple shape the actuation law can be easily implemented in the DNS code. The design of the feedback finaly is quite cheap considering that only two DNS and some computations on a ROM of low dimension (lower than 10) are required.

Let recall that the complexity of the numerical suite to get the actuation laws has not been realy described here, but numerous options and parameters need to be set carefully.

Chapter 2

Feedback control of acoustic waves with DNS and POD analysis

This chapter is concentrated on the analysis of the actuation law and of the actuated flow when the feedback control law is implemented in the Direct Numerical Simulations.

2.1 Actuation level and efficiency

The direct output feedback law is implemented in the full DNS code. Equation (1.9) shows that the control amplitude $\max|\gamma|$ depends on β which is a velocity. β is a function of the equilibrium state $\boldsymbol{a}^{\mathrm{e}}$ which in general is not unique. It is also related to the output identification matrix $\tilde{C}$: the sensor positions (Fig. 1.3) must lead to a good observability obtained from a Lyapunov equation [12]. The $\tilde{D}$ and K_c vector dependence means that the actuation mode must be representative of the physics, the state space system must therefore have a good controllability verified by a Lyapunov equation as well. Finally, the value of β is maximum when the control parameter ℓ goes to 0. When all conditions are fulfilled the control law produces a flow stabilization in the direct numerical simulations, otherwise exponential divergence occurs introduced by the components of α. With the chosen parameters, we find β=5.16 m/s (case A). From Fig. 2.1, we see that the amplitude of the actuation slowly decreases in time and the pressure fluctuations do the same. However the damping rate is quite small and a long time simulation is required to get a strong noise reduction of several decibels (a maximum of 3 dB after 45000 time steps). It is quite complex and time consuming to control the values of β and α by changing sensors' positions, actuation modes or by playing with the other parameters. So to improve the efficiency of actuation in the DNS, we propose to progressively increase the value of β in the control law (1.9) to 10.16 m/s (case B) and 17 m/s (case C). Here, only results of case C are discussed. For lower values of β, the conclusions are similar but the control effect is lower. For case C, the maximun actuation level in the flow field is around 8 $\%$ of the upstream velocity and generates weak nonlinearities. The damping of the control law in Fig. 2.1 indicates that efficiency is higher when $\gamma(t)$ is larger. The actuation seems to converge towards a constante value respectively of 3.56, 8.16 and 14.5 m/s for cases A to C. It indicates that the flow outputs $\boldsymbol{y}(t) - \bar{\boldsymbol{y}}$ converges towards a non zero constante value and the flow goes towards another stable state different from equilibrium state of the unactuated flow: the non zero wall steady asymptotic actuation is now a part of this new actuated equilibrium state.

The control law has been designed for a time period of 25 000 Δt but actuation remains efficient for longer time, far from the initial time window T_h (at least up to 80 000 Δt). The control law is quite robust but the quasi-perfect periodicity of the initial unactuated flow contributes to this result.

To go deeper into the flow analysis we have compared for the probes displayed in Fig. 1.4, the nondi-

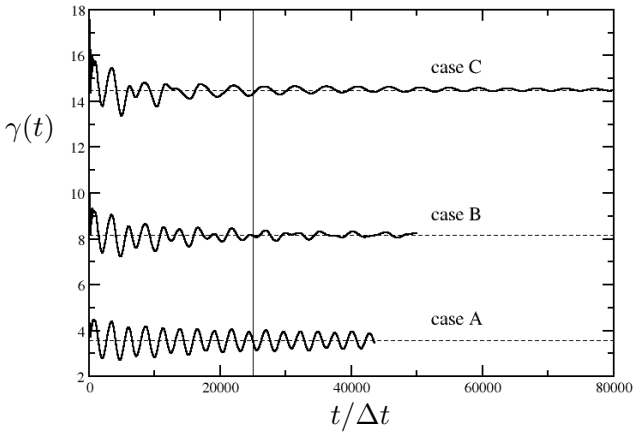

Figure 2.1 - *Forcing $\gamma(t)$ for three values of β and mean values.*

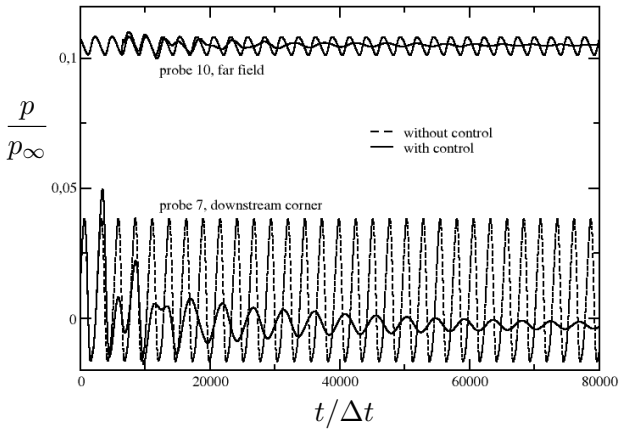

Figure 2.2 - *Time evolutions of pressure for the unactuated flow and case C.*

mensional pressure p/p_∞ obtained in case C with the unforced flow results. Some general trends are discussed now. In the main part of the computational domain, and especially in the emission zone and inside the directivity cone of the acoustic waves, the mean time pressure value has greatly decreased. In zones far upstream and far downstream the cavity, very close to the wall (probes 1, 2 and 8) the sound waves originated from the cavity are quasi unobservable and the mean pressure is greatly increased by the actuation perturbation. The Sound Pressure Level (SPL) has decreased globally except in some small localized area discussed later. Figure 2.2 displays signals obtained for some typical probes, one located in the vicinity of the downstream corner and of the sound source location (probe 7), and another one located in the far field (probe 10) that is more representative of the sound propagation.

Figure 2.3 demonstrates the control efficiency. Fast Fourier Transforms (FFT) of pressure's signals indicate that the control damps the fundamental frequency and its harmonics (a maximum of 1/8 approximately). A subharmonic has been generated by the actuation, a footprint of the weakly nonlinear effect.

2.2 Noise reduction, Sound Pressure Level

The global noise reduction is displayed in Fig. 2.4 through the difference of SPL between the actuated flow (case C) (left of fig. 2.5) and the unactuated flow (right of fig. 2.5). A damping of approximately 10 dB is reached close to the maximum of the SPL of the unactuated flow, in the shear layer and close to the downstream corner. On some localized and small zone located on the top of the cavity and downstream, the SPL has increased of several dB (up to 6 or more). Actually, the SPL level of the unactuated flow was really low and even with this amplification, the SPL remains low comparing to the mean SPL level as demonstrated on figure 2.5. The weakly nonlinear effect of the actuation on the flow is emphasized by the appearance of waves on some contours around -7 dB on figure 2.4 and which are not seen on figure 2.5. It could generated a secondary subharmonic instability (see Figure 2.3 as well) as it is well known in boundary layers or other flows but further investigations are necessary.

2.3 POD analysis of the actuated flow

It could be interested to carry out a Proper Orthogonal Decomposion following equation (1.2) of the actuated flow and to compare its new dynamics to those of the unactuated flow.

The figure 2.6 shows the Relative Information Content of the both flows. To get 99.99 % of the full energy, four modes are required in the unactuated flow while ten modes are not sufficient with actuation.

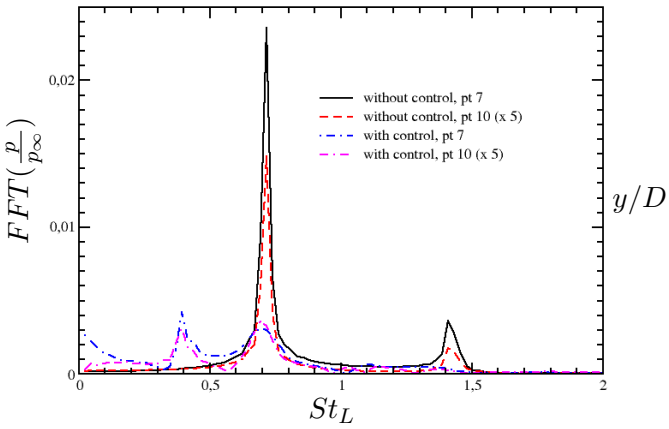

Figure 2.3 - *FFT of pressure signals. Comparisons between the unactuated flow and the controlled one (case C). The values of probe 10 are scaled by 5.*

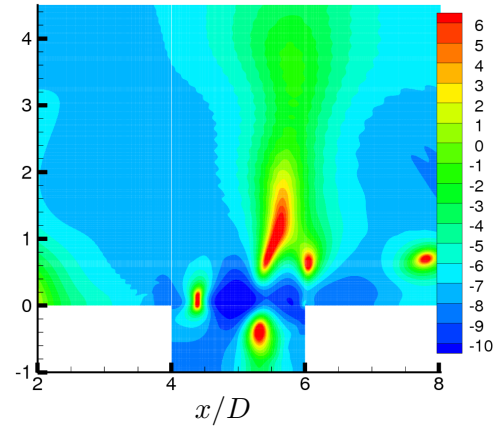

Figure 2.4 - *Difference of SPL between the unactuated flow and the controlled one (case C). Values in decibels (dB).*

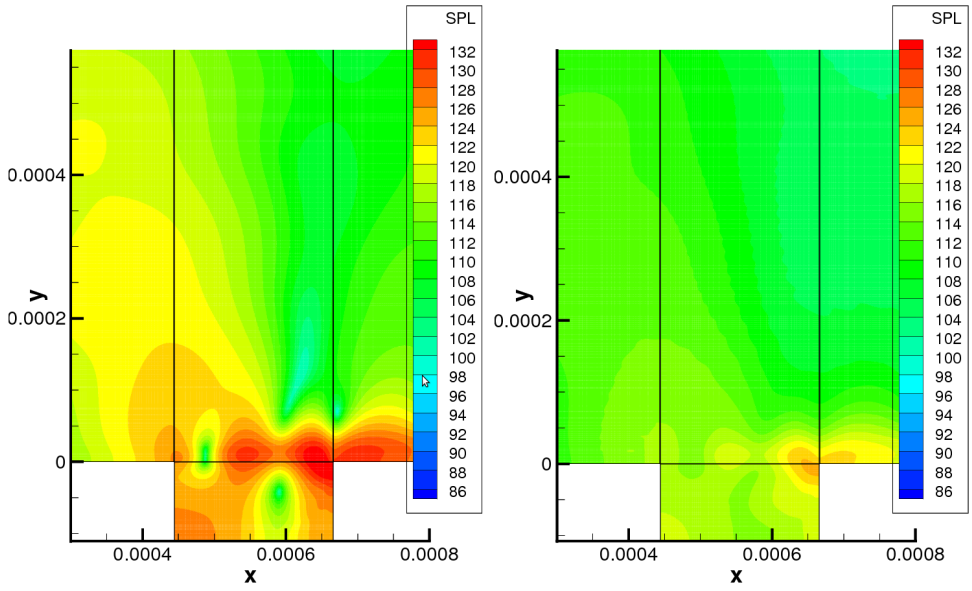

Figure 2.5 - *Sound Pressure Level of the unactuated and actuated flows*

The flow dynamics has been drastically complexified.

The mean perturbated pressure fields before and after actuation (the zeroth POD modes) ploted on figure 2.4 recall that the level of actuation is high enough to introduce a variation and therefore a non-linearity of the mean flow. It is therefore interesting to remind that the design of the actuation mode and the design of the actuation law was assuming a negligible nonlinear effect on the mean flow. It is another indicator of a certain robustness of the actuation law.

The phase portraits of the first five temporal coefficients are shown on figure 2.8. The curve for the unactuated flow are all closed (in red) because of the perfect time periodicy of the flow. However, for the unactuated flow, again the new flow dynamics is exhibited by large oscillations. For all phase portraits, we can guess that the curves will converge towards a fixed point. It is at least obvious for the coefficients a_2 versus a_1. It confirms that for infinite horizon, all flow fluctuations will be damped and the the flow will converge towards a steady new equilibrium state which can be determined asymptoticaly from the location of the fixed points in the phase portrait. This part requires more investigations however.

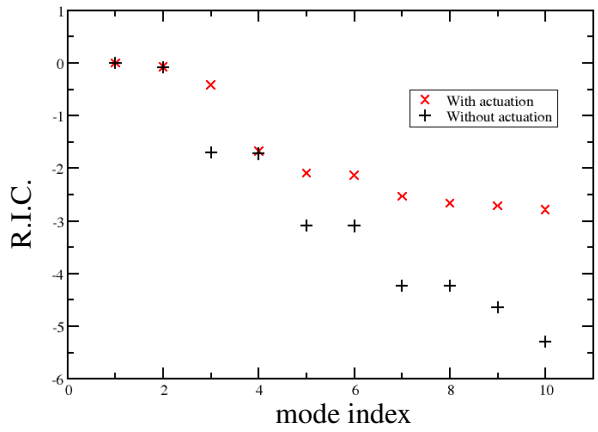

Figure 2.6 - *Relative Information Contents*

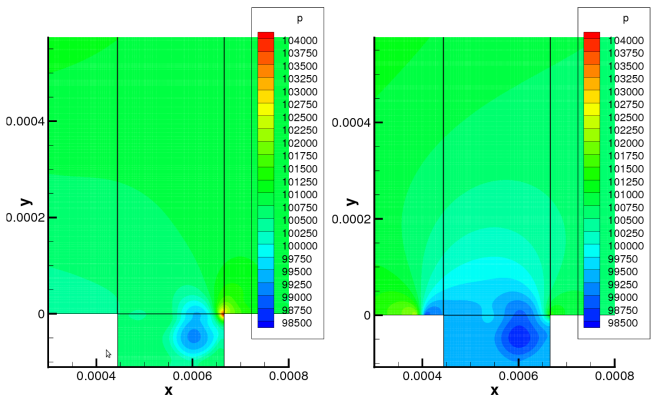

Figure 2.7 - *Mean pressure*

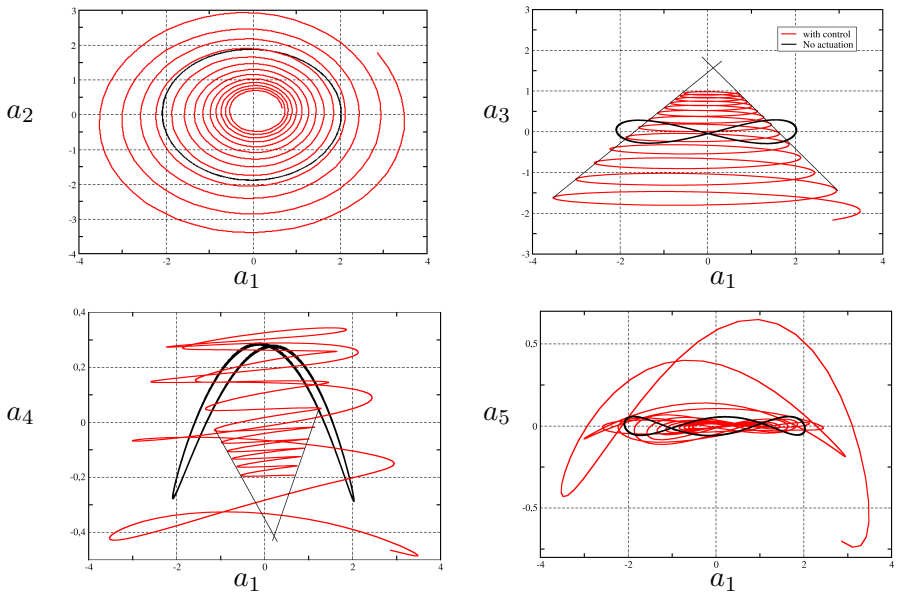

Figure 2.8 - *Phase portraits, in black: closed curves for unactuated flow, in red, convergente curves for actuated flow*

2.4 Summary

The efficient and in some way the robustness of the actuation law have been numerically proved. The linear property of the actuation law has allowed to use the constante β as a paremeter to improve the efficency of the control. As result the actuated flow seems to converge towards a new equilibrium state while the actuation law becomes steady for infinite time. Some weakly nonlinear effects are observed without perturbating the control efficiency.

Summary and future works

A global noise reduction, up to 10 dB, has been reached by implementing a direct output feedback actuation law into Direct Numerical Simulations, using a LQR strategy based on Reduced Order Modelling. The actuation law remains really efficient far after the time window used to design the law or by tuning the actuation by a constant value, which leads to some weak nonlinearities, proving its robustness.

Concerning computational resources, the proposed approach requires only two DNS for determining the actuation mode, and then rests only on reduced-order models. Compared to an optimal open-loop control approach or to an optimization strategy for which many DNS simulations have to be done, our approach is really cheaper.

As current works, we no longer use a LQR control approach. We improve the former Linear Quadratic Gaussian control implementation in the ROM by proposing a feedback law given by a convolution product :

$$\gamma(t) = \int_{t-t_c}^{t} \sum_{i=1}^{N_s} G_i(t-\tau)\boldsymbol{y}_i(\tau)\, d\tau$$

t_c is a delayed time which allows to have the history of the flow in the actuation law. This more complex actuation law can take into account of the noise or uncertainties associated to sensors and the actuators.

As the perspectives, more investigations are necessary to take into account of the actuation mode in the ROM. For instance we could add the actuation time derivative as it is done by some authors. Another possibility is to activate simultaneoustly several actuators at several positions.

The robusness can be as well enhance by using H_2 and H_∞ control in the ROM but as well by designing and testing actuation law in some given range of Reyndols numbers and Mach numbers.

Moreover, the general control efficiency could be enhanced by going further towards nonlinear flow control.

The last but probably most important issue would be to define a wind tunnel experiment to control for instance separation at relative low Mach number and Reynolds number and to use the DNS and this methodology to propose and to test various feedback law depending on actuators positions and types and on sensors positions.

Acknowledgments

This work has been supported by the Fondation de la Recherche pour l'Aéronautique et l'Espace (FRAE) under the ECOSEA project. We would also like to thank the CALMIP center in Toulouse for providing the computational resources.

This work is another brick inside a complex association of various numerical tools and various theories. So I would like to thanks all people (colleagues, students) and financial supports who helped me during at least the last decade.

Appendix

A-Inner product

a) Variance inner product

On introducing $\boldsymbol{q} = (\zeta, u, v, p)$ with $\zeta = 1/\rho$ and for non-dimensional variables we have:

$$\langle \boldsymbol{q}_1, \boldsymbol{q}_2 \rangle_\Omega = \int_\Omega \left(\alpha_\zeta \zeta_1 \zeta_2 + \alpha_u u_1 u_2 + \alpha_v v_1 v_2 + \alpha_p p_1 p_2\right) d\Omega$$

In the inner product, the weight α_μ are the inverse of the square of the variance of the variable μ :

$$\alpha_\mu = 1/\sigma^2(\mu), \qquad \text{where} \qquad \sigma^2(\mu) \;=\; \int_\Omega \frac{1}{T} \int_0^T \left(\mu(\mathbf{x}, t) - \bar{\mu}(\mathbf{x})\right)^2 \, dt \, d\Omega \tag{1}$$

$\bar{\mu}$ is the temporal mean value of μ on the time interval $[0\ T]$.

b) Energy based inner product

For the case of compressible flows, the velocity variables are dynamically coupled with the thermodynamic variables. The inner product which defined the correlation tensor adds the flow variables and the thermodynamic variables. A question arises when we add two variables of different dimensions to make sense when we use the usual L^2 inner product. The scalar inner product can be computed for each variable as it has been used by [18].

For vector valued variables one choice could be to non-dimensionalize the variables, but the meaning of non-dimensionalization on the optimality of the projections is not clear. [18] seeks an inner product, for the isentropic flow variables can be interpreted as an energy. This inner product has been used widely to study cold isentropic flows at low Mach numbers by [19], [8].The vector variable is defined with $\boldsymbol{q} = (u, v, c)$, where u and v are flow variables and c the local speed of sound. The inner product is then written.

$$\langle q_1, q_2 \rangle = \int_\Omega \left(u_1 u_2 + v_1 v_2 + \frac{2\alpha}{\gamma - 1} c_1 c_2 \right) d\Omega \tag{2}$$

where γ is the ratio of specific heats and α is a parameter to be chosen. $\alpha = 1$, respectively $\alpha = 1/\gamma$ corresponds to the integration of the stagnation enthalpy and respectively of the stagnation energy [8].

.

B-ROM with the $1/\rho$ formulation

Galerkin projection

The low-order model of the full Navier-Stokes equation has cubical implicit terms,Vigo suggests the use of a formulation by using the primitive variables (u, v, p) and the specific volume $\zeta = \frac{1}{\rho}$. The fully compressible Navier-Stokes equation in terms of these variables can be written as:

$$\begin{array}{rcl} \zeta_t & = & \zeta(u_x + v_y) - u\zeta_x - v\zeta_y \\ u_t & = & -uu_x - vu_y - \zeta p_x + \frac{1}{Re}\zeta\left[\left(\frac{4}{3}u_x - \frac{2}{3}v_y\right)_x + (v_x + u_y)_y\right] \\ v_t & = & -uv_x - vv_y - \zeta p_y + \frac{1}{Re}\zeta\left[\left(\frac{4}{3}v_y - \frac{2}{3}u_x\right)_y + (v_x + u_y)_x\right] \\ p_t & = & -up_x - vp_y - \gamma p(u_x + v_y) + \frac{\gamma}{RePr}[(p\zeta)_{xx} + (p\zeta)_{yy}] \\ & + & \frac{\gamma-1}{Re}\left[u_x\left(\frac{4}{3}u_x - \frac{2}{3}v_y\right) + v_y\left(\frac{4}{3}v_y - \frac{2}{3}u_x\right) + (v_x + u_y)^2\right] \end{array} \tag{3}$$

On introducing $q = (\zeta, u, v, p)$ the above equation can be re-casted as

$$\dot{q} = \mathcal{Q}_1(q, q) + \frac{1}{Re}\mathcal{Q}_2(q, q) \tag{4}$$

with

$$\mathcal{Q}_1(q_1, q_2) = -\begin{pmatrix} u_1\zeta_{2x} + v_1\zeta_{2y} - \zeta_1(u_{2x} + v_{2y}) \\ u_1u_{2x} + v_1u_{2y} + \zeta_1 p_{2x} \\ u_1v_{2x} + v_1v_{2y} + \zeta_1 p_{2y} \\ u_1p_{2x} + v_1p_{2y} + \gamma p_1(u_{2x} + v_{2y}) \end{pmatrix}$$

$$\mathcal{Q}_2(q_1, q_2) = \begin{pmatrix} 0 \\ \zeta_1\left[\left(\frac{4}{3}u_{2x} - \frac{2}{3}v_{2y}\right)_x + (v_{2x} + u_{2y})_y\right] \\ \zeta_1\left[\left(\frac{4}{3}v_{2y} - \frac{2}{3}u_{2x}\right)_y + (v_{2x} + u_{2y})_x\right] \\ Q_3 \end{pmatrix}$$

$$\begin{array}{rcl} Q_3 & = & \frac{\gamma}{Pr}[(p_2\zeta_1)_{xx} + (p_2\zeta_1)_{yy}] + (\gamma - 1)\left[u_{1x}\left(\frac{4}{3}u_{2x} - \frac{2}{3}v_{2y}\right)\right. \\ & + & \left. v_{1y}\left(\frac{4}{3}v_{2y} - \frac{2}{3}u_{2x}\right) + (v_{1x} + u_{1y})(v_{2x} + u_{2y})\right] \end{array}$$

Actuated nonlinear dynamical system

By taking into account of the actuation mode ψ^* in the Galerkin projection of the Navier-Stokes equation on the POD modes,an actuated nonlinear dynamical system can be written as :

$$\dot{a}_i = \sum_{j=1}^{N}(L_{1ij} + \frac{L_{2ij}}{Re} + \gamma(t)h_{2ij})a_j + \sum_{j,k=1}^{N}(Q_{1ijk} + \frac{Q_{2ijk}}{Re})a_ja_k + \gamma(t)h_{1i} + \gamma(t)^2h_{3i}$$

where

$$
\begin{aligned}
h_{1i} &= \langle \mathcal{Q}_1(\psi^*, \bar{q}) + \mathcal{Q}_1(\bar{q}, \psi^*), \phi_i \rangle_\Omega + \frac{1}{Re} \langle \mathcal{Q}_2(\psi^*, \bar{q}) + \mathcal{Q}_2(\bar{q}, \psi^*), \phi_i \rangle_\omega \\
h_{2ij} &= \langle \mathcal{Q}_1(\psi^*, \phi_j) + \mathcal{Q}_1(\phi_j, \psi^*), \phi_i \rangle_\omega + \frac{1}{Re} \langle \mathcal{Q}_2(\psi^*, \phi_j) + \mathcal{Q}_2(\phi_j, \psi^*), \phi_i \rangle_\omega \\
h_{3i} &= \langle \mathcal{Q}_1(\psi^*, \psi^*), \phi_i \rangle_\omega + \frac{1}{Re} \langle \mathcal{Q}_2(\psi^*, \psi^*), \phi_i \rangle_\omega
\end{aligned}
$$

C-Unactuated and actuated ROM - Calibration

The first inner product used to get POD spatial modes and time coefficients was the one based on the energy (eq. 2). To get the reduced order model, we used the isentropic equation in the Galerkin projection similarly to [8]. In the figures 9 and 10 this case is referred as "Isen". Then we used the inner product based on the variance (eq. 1) and the equations 3 was used in the Galerkin projection. This case is referred as "Vigo" in the figures. The figure 10a) shows that the POD coefficient $a_1(t)$ are very similar and so far inner-product independent, except that the amplitude level are not equal because of the POD spatial mode normalization. The conclusion is the same for the other time coefficients of interest. The next figures 10b) to 10c) show the comparison of the three first time coefficients. As expected, the coefficients obtained from the time integration of the ROM are unstable, but they seems more accurate in comparison with the POD reference coefficients in the Vigo's case. That let us think that it was necessary to choose this later inner product and the Navier-Stokes equations in the Galerkin projection for control purpose. Naturally, after the calibration process, the time coefficients given from the ROM time integration perfectly match with the reference.

In the figure 10 are compared the $a_1(t)$ coefficients before the calibration process, in four case : unactuated POD, unactuated ROM with Vigo's formulation, with the chirp actuation and the isentropic model and with the chirp actuation and the Vigo's formulation. The conclusion is quite obvious, the use of the Vigo's formulation is a great improvement to better take into account of the actuation in the nonlinear dynamical system.

D-ANR Cormored / Ecosea project tasks

The Ecosea project lead to large significant improvement from the ANR Cormored project.

Topic	Cormored	Ecosea
DNS		Implementation of the feedback law
Adjoint DNS	Implementation	Calculus
ROM	inner product based on energy	Inner product based on variance
ROM	Isentropic model	Vigo's model (Navier-Stokes model)
Estimation	$\tilde{\mathbf{p}} = \tilde{C}\boldsymbol{a}$	$\tilde{\mathbf{p}} = \tilde{C}\boldsymbol{a} + D\gamma$
Control law	LQG implementation	LQR + direct output feedback law implemeted in the DNS

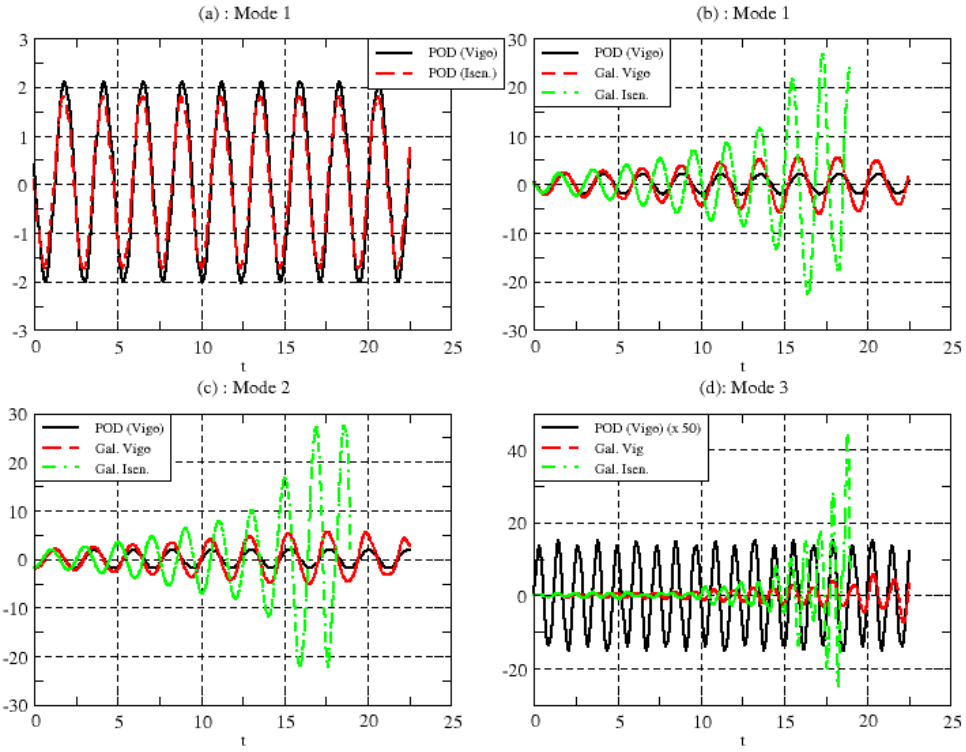

Figure 9 - $a_k(t)$, $k = 1..4$. *Comparisons of the time integration coefficients of the unactuated ROM obtained by two inner products, the one associated on the isentropic model (Isen) and the variance inner product associated to the Navier-Stokes equation in Vigo's formulation*

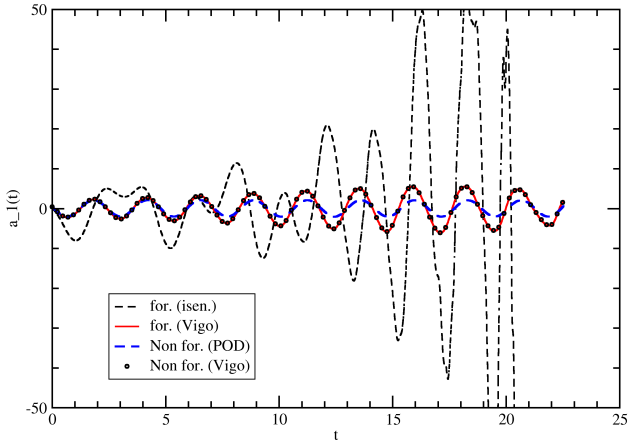

Figure 10 - $a_1(t)$ *coefficient versus time. Comparisons of the integration of the ROM, in unactuatted and actuated situation, the reference is the* $a_1(t)$ *given by the POD*

Bibliography

[1] AHUJA, S., AND ROWLEY, C. W. Feedback control of unstable steady states of flow past a flate plate using reduced-order estimators. *J. Fluid Mech. 645* (2010), 447–478. 5

[2] AHUJA, S., AND ROWLEY, C. W. Feedback control of cavity flow oscillations using simple linear models. *J. Fluid Mech. 709* (2012), 223–248. 5

[3] AIRIAU, C. Noise sensitivity in a 2D compressible boundary layer flow past a cavity. In $20^{ème}$ *Congrès Français de Mécanique* (Besançon, France, August 2011). http://www.femto-st.fr/f/d/ActesCFM2011.pdf. 7

[4] BARBAGALLO, A., SIPP, D., AND SCHMID, P. Closed-loop control of an open cavity flow using reduced-order model. *J. Fluid Mech. 641* (2009), 1–50. 5

[5] BARBAGALLO, A., SIPP, D., AND SCHMID, P. Feedback control of unstable steady states of flow past a flate plate using reduced-order estimators. *J. Fluid Mech. 685* (2011), 23–53. 5

[6] BOURGUET, R., BRAZA, M., SVRAIN, A., AND BOUHADJI, A. Capturing transition features around a wing by reduced-order modeling based on compressible Navier-Stokes equations. *Phys. Fluids 21*, 094104 (2009), 1–11. 8, 9

[7] CORDIER, L., NOACK, B. R., TISSOT, G., LEHNASCH, G., DELVILLE, J., BALAJEWICZ, M., DAVILLER, G., AND NIVEN, R. Identification strategies for model-based control. Exp. in Fluids, *special issue Flow Control 54* (2013). 10

[8] GLOERFELT, X. Compressible Proper Orthogonal Decomposition/Galerkin reduced order model of self sustained oscillations in a cavity. *Phys. Fluids 20* (2008). 18, 20

[9] KASNAKOĞLU, C. *Reduced Order Modeling, nonlinear analysis and control methods for flow control.* PhD thesis, Ohio State University, 2007. 5, 8

[10] KLOKER, M. J. A robust high-resolution split-type compact FD scheme for spatial direct numerical simulation of boundary-layer transition. *Applied Scientific Research 59* (1998), 353–377. 7

[11] LELE, S. K. Compact finite difference schemes with spectral-like resolution. *J. Comput. Phys. 103* (1992), 16–42. 7

[12] LEWIS, F., VRABIE, D., AND SYRMOS, V. *Optimal control*. Third edition. Wiley, 2012. 12

[13] MORET, L. *Aeroacoustic investigation and adjoint analysis of subsonic cavity flows*. PhD thesis, Université de Toulouse, INPT, Toulouse, France, November 2009. 6, 7

[14] NAGARAJAN, K., CORDIER, L., AND AIRIAU, C. Development and Application of a Reduced Order Model for the Control of Self-Sustained Instabilities in Cavity Flows. *Commun. Comput. Phys. 14* (2013), 186–218. 5, 6, 8, 10

[15] NOACK, B., MORZYNSKI, M., AND TADMOR, G. *Reduced-Order Modelling for Flow Control*, vol. 528 of *CISM Courses and Lectures 528*. Springer-Verlag, 2010. 8

[16] POINSOT, T. J., AND LELE, S. K. Boundary conditions for direct simulations of compressible viscous flows. *J. Comput. Phys. 101* (1992), 104–129. 7

[17] ROSSITER, J. Wind-tunnel experiments on the flow over rectangular cavities at subsonic and transonic speeds. Tech. Rep and Memoranda 3438, Aeronautical Research Council, 1964. 6

[18] ROWLEY, C. *Modeling, Simulation, and Control of Cavity Flow Oscillations*. PhD thesis, California Institute of Technology, 2001. 18

[19] ROWLEY, C., COLONIUS, T., AND MURRAY, R. Model reduction of compressible flows using POD and Galerkin projection. *Physica D 189* (2003), 115–129. 18

[20] ROWLEY, C. W., COLONIUS, T., AND BASU, A. J. On Self-sustained Oscillations in two-dimensional Compressible Flow over Rectangular Cavities. *J. Fluid Mech. 455* (2002), 315–346. 6

[21] SPAGNOLI, B., AND AIRIAU, C. Adjoint analysis for noise control in a two-dimensional compressible mixing layer. *Computers and Fluids 37* (2008), 475–486. 7

[22] THOMPSON, K. W. Time dependent boundary conditions for hyperbolic systems ii. *J. Comput. Phys. 89* (1990), 439–561. 7

[23] VIGO, G. La décomposition orthogonale propre appliquée aux équations de navier-stokes compressibles instationnaires . Tech. Rep. 3385, INRIA, 1998. 9